



**HAL**  
open science

## Conservative numerical methods for the Full von Kármán plate equations

Stefan Bilbao, Olivier Thomas, Cyril Touzé, Michele Ducceschi

► **To cite this version:**

Stefan Bilbao, Olivier Thomas, Cyril Touzé, Michele Ducceschi. Conservative numerical methods for the Full von Kármán plate equations. *Numerical Methods for Partial Differential Equations*, 2015, 31 (6), 10.1002/num.21974 . hal-01206323

**HAL Id: hal-01206323**

**<https://ensta-paris.hal.science/hal-01206323>**

Submitted on 14 Mar 2016

**HAL** is a multi-disciplinary open access archive for the deposit and dissemination of scientific research documents, whether they are published or not. The documents may come from teaching and research institutions in France or abroad, or from public or private research centers.

L'archive ouverte pluridisciplinaire **HAL**, est destinée au dépôt et à la diffusion de documents scientifiques de niveau recherche, publiés ou non, émanant des établissements d'enseignement et de recherche français ou étrangers, des laboratoires publics ou privés.

# Conservative Numerical Methods for the Full von Kármán Plate Equations

Stefan Bilbao

*Acoustics and Audio Group  
James Clerk Maxwell Building  
King's Buildings  
University of Edinburgh  
Mayfield Rd., Edinburgh  
EH9 3JZ United Kingdom  
Tel.: +44 (0)131 651 7043  
Fax: +44 (0) 131 650 2425  
Email: sbilbao@staffmail.ed.ac.uk*

Olivier Thomas

*Arts et Métiers ParisTech  
LSIS UMR CNRS 7296  
8 bd. Louis XIV  
59046 Lille, France*

Cyril Touzé and Michele Ducceschi

*IMSIA (Institute of Mechanical Sciences and Industrial Applications)  
UMR 8193 CNRS-EDF-CEA-ENSTA  
Université Paris-Saclay  
828 Boulevard des Maréchaux  
81762 Palaiseau Cedex, France.*

This article is concerned with the numerical solution of the full dynamical von Kármán plate equations for geometrically nonlinear (large-amplitude) vibration in the simple case of a rectangular plate under periodic boundary conditions. This system is composed of three equations describing the time evolution of the transverse displacement field, as well as the two longitudinal displacements. Particular emphasis is put on developing a family of numerical schemes which, when losses are absent, are exactly energy conserving. The methodology thus extends previous work on the simple von Kármán system, for which longitudinal inertia effects are neglected, resulting in a set of two equations for the transverse displacement and an Airy stress function. Both the semi-discrete (in time) and fully discrete schemes are developed. From the numerical energy conservation property, it is possible to arrive at sufficient conditions for numerical stability, under strongly nonlinear conditions. Simulation results are presented, illustrating various

features of plate vibration at high amplitudes, as well as the numerical energy conservation property, using both simple finite difference as well as Fourier spectral discretisations.

## I. INTRODUCTION

Thin plates and shells vibrating at large amplitude display geometric nonlinearity when the vibration amplitude is at least of the order of the thickness. Various interesting nonlinear phenomena are exhibited which can be classified according to the amplitude of the nonlinear vibration.

- For weakly nonlinear vibrations in the low-frequency part of the eigenspectrum, jump phenomena and hysteresis due to Duffing-like responses are well documented [1, 2, 3]. Mode coupling and energy exchange between internally resonant modes is a second common feature, now well established in the literature [4, 5, 6, 7, 8, 9, 10, 11].
- Under strongly nonlinear conditions, a transition to a chaotic or wave turbulent regime is observed. This transition scenario is documented in [12, 13, 14], while spatio-temporal dynamics [15] and the existence of inertial manifolds and attractors are mathematically demonstrated in [16, 17].
- In the strongly nonlinear or wave turbulent regime, an energy cascade from the injection to the dissipative scale has been recently demonstrated theoretically [18], and then studied experimentally [19, 20, 21] and numerically [18, 22, 23, 24, 25].

Most work on the nonlinear dynamics of thin plates uses the von Kármán assumptions, which introduce a particular truncation in the strain-displacement relationship [26, 27, 28, 29]. More specifically, a simplified version of the von Kármán plate equations is used, where in-plane inertia is neglected, such that an Airy stress function can be used to describe in-plane motion. This approximation was first introduced by Föppl [30, 31, 32] and the simplified model is often referred to as the Föppl-von Kármán system. In this contribution, this model will be named the simple von Kármán system. It is known to give good results in the moderately nonlinear regime, and in the low-frequency part of the eigenspectrum of the plate. However, in recent studies, numerical simulations are carried out up to a vibration amplitude that is 5 to sometimes 10 times the thickness, or, in the context of wave turbulence, down to small wavelengths where in-plane inertia may play a role [11, 23, 24]. Very few studies are available for checking the validity limits of the simple von Kármán plate model versus a full von Kármán system where in-plane inertia is retained, or versus more complex models including for example rotatory inertia or shear effects, following *e.g.* Reissner-Mindlin kinematics. To our knowledge one article covers this subject for plates [33], where the dynamic response of simple, full and fully three-dimensional plate equations are compared in particular cases. The paper showed clearly that the simple von Kármán model is a very good approximation when the thickness is smaller than 1/20 of other typical dimensions (such as a side length) [33]. However the number of dynamical solutions simulated is scarce, and the high-frequency range was not tested so that other simulations are still needed in order to have a better picture of the validity limit of the model. Note that for shells, where a variety of simplified models are also available, a comparative study is provided in [34], but only in the vicinity of the first eigenfrequencies.

Numerical simulation approaches to the study of plate vibrations have taken on a variety of different forms. Some have involved nonlinear coupled modal descriptions, using a Galerkin-based formulation with eigenmodes as a functional basis [4, 7, 11] or an ad-hoc functional basis having good properties [9]. Finite difference methods have been successfully used in [35]. Finite element approaches have also been used (see *e.g.* [36, 37, 38, 39]), as well as spectral and pseudo-spectral methods [40, 33, 18, 23, 24]. In most cases, the spatial part of the problem is solved first, and then the solution advanced in time through a standard time discretization procedure, such as, *e.g.*, leap frog, or one of the Runge Kutta families of schemes [15, 40, 18].

In parallel, the last two decades have seen an increasing interest in defining conservative schemes, *i.e.* time-stepping methods where the conservation of invariants such as, *e.g.*, the discrete energy is an in-built property [41, 42, 43]. General procedures for Hamiltonian wave equations by McLachlan [44]. These methods are of great utility as a means of ensuring stability even under highly nonlinear conditions, and particularly in examining the transition to the wave turbulent regime, and indeed spectral characteristics of the fully wave turbulent regime. For the simple von Kármán plate model, a family of energy-conserving schemes has been derived in [35].

The goal here is to introduce conservative schemes for the full von Kármán plate model where in-plane inertia is retained, in a comparative manner to the developments for the simplified system reported in [35]. This paper is organized as follows: In Section II., the full von Kármán system is presented, in the case of a rectangular plate under periodic boundary conditions, accompanied by a brief energy analysis. Semi-discrete parameterized families of time stepping methods, with an inherent energy conservation property are introduced in Section III.; such methods are suitable for full discretization by a variety of means. To this end, in Section IV., several examples of full discrete methods, including both simple finite difference schemes, and Fourier spectral discretisation, are discussed accompanied by stability analysis, following from an energy conservation property in the fully discrete case. Such methods are distinct from those arrived at through separate spatial and temporal discretisation. Simulation results are presented in Section V. For the sake of completeness, the addition of rotatory inertia and loss terms is covered in the Appendix.

## II. MODEL: FULL VON KÁRMÁN SYSTEM

The full von Kármán system, describing transverse and in-plane large amplitude vibration of a flat plate, has been presented by various authors [45, 46, 47, 48]. In nondimensional form, it may be written as

$$\ddot{\mathbf{u}} - \operatorname{div} \mathbf{N} = 0 \quad (2.1a)$$

$$\ddot{w} - \operatorname{div} \operatorname{div} \mathbf{M} - \operatorname{div} (\mathbf{N} \nabla w) = 0 \quad (2.1b)$$

$$\mathbf{M} = -\phi(\nabla \nabla w) \quad (2.1c)$$

$$\mathbf{N} = \phi(\boldsymbol{\epsilon}) \quad (2.1d)$$

$$\boldsymbol{\epsilon} = \frac{1}{2} (\nabla \mathbf{u} + \nabla \mathbf{u}^T + \nabla w \otimes \nabla w) \quad (2.1e)$$

where here,  $w(x, y, t)$  is transverse displacement and  $\mathbf{u}(x, y, t) = [u(x, y, t), v(x, y, t)]^T$  is the in-plane displacement vector; both are functions of spatial coordinates  $x$  and  $y$  and

time  $t$ . Dots indicate time differentiation, and the operator  $\nabla$  is the gradient in 2D. The problem is assumed defined for  $t \in \mathbb{R}^+$ , and over a domain  $(x, y) \in \Omega \subset \mathbb{R}^2$ .  $\mathbf{M}$  and  $\mathbf{N}$  are the bending moment and membrane force tensors, respectively.

The independent and dependent variables may be related to their dimensional counterparts (with overbars) through the scalings

$$(\bar{x}, \bar{y}) = r_0(x, y) \quad \bar{\mathbf{u}} = r_0 \mathbf{u} \quad \bar{w} = r_0 w \quad \bar{t} = r_0 \sqrt{\frac{\rho H}{A}} t \quad \bar{\mathbf{M}} = AH\mathbf{M} \quad \bar{\mathbf{N}} = AN \quad (2.2)$$

Here,  $\rho$  is density and  $H$  is thickness, both assumed constant here. The membrane stiffness  $A$  is defined as  $A = EH/(1 - \nu^2)$  in terms of  $H$ , Young's modulus  $E$ , and Poisson's ratio  $\nu$ . The constant  $r_0$  is defined as  $r_0 = H/\sqrt{12}$ .

The tensors  $\mathbf{M}$  and  $\mathbf{N}$  are defined in terms of a general  $2 \times 2$  tensor mapping  $\mathbf{F} \rightarrow \phi(\mathbf{F})$ :

$$\phi(\mathbf{F}) = \nu \text{tr}(\mathbf{F}) \mathbf{1} + (1 - \nu) \mathbf{F} \quad (2.3)$$

where  $\mathbf{1}$  indicates the  $2 \times 2$  identity matrix and  $\text{tr}(\cdot)$  is the trace operation. See, e.g., [49]. The tensor gradient  $\nabla$  and product  $\otimes$  are defined, in terms of functions  $\mathbf{f} = [f_x, f_y]^T$  and  $\mathbf{g} = [g_x, g_y]^T$  as

$$\nabla \mathbf{f} = \begin{bmatrix} \frac{\partial f_x}{\partial x} & \frac{\partial f_x}{\partial y} \\ \frac{\partial f_y}{\partial x} & \frac{\partial f_y}{\partial y} \end{bmatrix} \quad \mathbf{f} \otimes \mathbf{g} = \begin{bmatrix} f_x g_x & f_x g_y \\ f_y g_x & f_y g_y \end{bmatrix} \quad (2.4)$$

$\epsilon$  is the mid-plane strain tensor, which is symmetric.

Note in particular that  $\text{div div } \mathbf{M} = -\Delta \Delta w$ , leading to the usual linear term involving the biharmonic operator in thin linear (Kirchhoff) models of plate vibration [50].

The assumptions underlying this model are that:

- a Kirchhoff-Love kinematic is assumed, where any normal to the plate mid-surface before deformation remains normal to the deformed mid-surface. The transverse shear stresses are thus neglected;
- normal stresses along the transverse directions are neglected;
- the von Kármán-like strain-displacement law of (2.1d) is used, by neglecting non-linear terms of higher order in the plane part of the Green-Lagrange strain tensor;
- the material is linear, homogeneous and isotropic;
- rotatory inertia terms are neglected.

Under further assumptions, namely that in-plane inertia terms may be neglected, it is possible to arrive at a simplified form of the von Kármán system, written in terms of transverse displacement  $w$  alone and a scalar function (often referred to as the Airy stress function). Conservative methods for this simplified system have been presented previously by one of the authors [35]. The rotatory inertia term may be reintroduced here with little difficulty, but is neglected here for simplicity—see the Appendix for a discussion of the addition of this effect along with loss terms.

#### A. Boundary Conditions

In this article, concerned with general strategies for the design of time-dependent update schemes for system (2.1), the system is assumed defined over a closed square region of nondimensional side-length  $L$ :

$$\Omega = \{(x, y) \in [0, L] \times [0, L]\} \quad (2.5)$$

and the boundary conditions are assumed to be of periodic type, by imposing that all displacements, slopes, force resultants and moments at the  $x = 0$  ( $y = 0$ ) edge are the same than those at the edge  $x = L$  ( $y = L$ ). Such periodic boundary conditions are often used in studies of wave turbulence [18, 22, 23]. In the discrete setting, over regular grids, such boundary conditions are easily implemented using periodic difference operations, which reduce to circulant matrix forms when such schemes are vectorized.

### B. Inner Products

For two functions  $\mathbf{F}(x, y, t)$  and  $\mathbf{G}(x, y, t)$  representing general scalar/vector/tensor fields, an  $L^2$  spatial inner product over  $\Omega$  is defined as

$$\langle \mathbf{F}, \mathbf{G} \rangle = \iint_{\Omega} \mathbf{F} \diamond \mathbf{G} d\Omega, \quad (2.6)$$

where  $\diamond$  is the standard product in the case of scalar fields, the standard dot-product in the case of vector fields and  $\mathbf{F} \diamond \mathbf{G} = \text{tr}(\mathbf{F}^T \mathbf{G})$  in the case of tensor fields ( $\text{tr}(\cdot)$  indicates the trace operation and  $^T$  the transpose operation). The norm of such a field  $\mathbf{F}$  is defined as

$$\|\mathbf{F}\| = \langle \mathbf{F}, \mathbf{F} \rangle^{1/2} \quad (2.7)$$

### C. Identities: Time Differentiation

For tensor (or scalar or vector)  $\mathbf{F}$  and  $\mathbf{G}$ ,

$$\frac{d}{dt} \langle \mathbf{F}, \mathbf{G} \rangle = \langle \dot{\mathbf{F}}, \mathbf{G} \rangle + \langle \mathbf{F}, \dot{\mathbf{G}} \rangle \quad \text{and} \quad \frac{d}{dt} \frac{1}{2} \|\mathbf{F}\|^2 = \langle \mathbf{F}, \dot{\mathbf{F}} \rangle \quad (2.8)$$

where  $d/dt$  indicates a total derivative of a scalar quantity, and where the dot notation indicates partial differentiation with respect to  $t$ .

### D. Identities: Integration by Parts

For scalar functions  $f$  and  $g$  defined over the periodic domain  $\Omega$ , integration by parts holds as follows:

$$\langle f, \Delta g \rangle = -\langle \nabla f, \nabla g \rangle \quad (2.9a)$$

$$\langle f, \Delta \Delta g \rangle = \langle \Delta f, \Delta g \rangle \quad (2.9b)$$

Here,  $\Delta(\cdot) = \text{div}(\nabla \cdot)$  is the Laplacian operator in 2D.

For vector (resp. scalar)  $\mathbf{f}$  and tensor (resp. vector)  $\mathbf{G}$ , integration by parts may be written as

$$\langle \mathbf{f}, \text{div} \mathbf{G} \rangle = -\langle \nabla \mathbf{f}, \mathbf{G} \rangle \quad (2.10)$$

### E. Identities: Tensors

For vectors  $\mathbf{f}$  and  $\mathbf{h}$  and tensor  $\mathbf{G}$ , it is true that

$$\mathbf{f} \diamond (\mathbf{G}\mathbf{h}) = (\mathbf{f} \otimes \mathbf{h}) \diamond \mathbf{G} \quad \implies \quad \langle \mathbf{f}, \mathbf{G}\mathbf{h} \rangle = \langle \mathbf{f} \otimes \mathbf{h}, \mathbf{G} \rangle \quad (2.11)$$

For a tensor  $\mathbf{F}$  and a symmetric tensor  $\mathbf{G}$ , it is true that

$$\mathbf{F} \diamond \mathbf{G} = \frac{1}{2} (\mathbf{F} + \mathbf{F}^T) \diamond \mathbf{G} \quad \implies \quad \langle \mathbf{F}, \mathbf{G} \rangle = \left\langle \frac{1}{2} (\mathbf{F} + \mathbf{F}^T), \mathbf{G} \right\rangle \quad (2.12)$$

F. Properties of the mapping  $\phi(\mathbf{F})$ 

The mapping  $\phi(\mathbf{F})$  preserves symmetry:

$$\mathbf{F} = \mathbf{F}^T \quad \Longrightarrow \quad \phi(\mathbf{F}) = \phi(\mathbf{F})^T \quad (2.13)$$

This property follows from the definition of the mapping  $\phi(\mathbf{F})$  from (2.3) in terms of the identity and  $\mathbf{F}$  itself.

The mapping  $\phi(\mathbf{F})$  satisfies a non-negativity property:

$$\phi(\mathbf{F}) \diamond \mathbf{F} = \nu (\text{tr}(\mathbf{F}))^2 + (1 - \nu) \mathbf{F} \diamond \mathbf{F} \geq 0 \quad \text{when} \quad 0 \leq \nu \leq 1 \quad (2.14)$$

(Note that in the present application,  $\nu$ , representing Poisson's ratio, satisfies  $0 \leq \nu \leq 1/2$ .) This property extends to the inner product as

$$\langle \mathbf{F}, \phi(\mathbf{F}) \rangle = \nu \|\text{tr}(\mathbf{F})\|^2 + (1 - \nu) \|\mathbf{F}\|^2 \quad (2.15)$$

Using the identity  $\mathbf{F} \diamond \phi(\mathbf{G}) = \phi(\mathbf{F}) \diamond \mathbf{G}$ , the following time differentiation identity also holds:

$$\langle \dot{\mathbf{F}}, \phi(\mathbf{F}) \rangle = \frac{d}{dt} \frac{1}{2} \langle \mathbf{F}, \phi(\mathbf{F}) \rangle \quad (2.16)$$

## G. Energy

Taking the vector inner product of (2.1a) with  $\dot{\mathbf{u}}$  gives:

$$\langle \dot{\mathbf{u}}, \ddot{\mathbf{u}} \rangle - \langle \dot{\mathbf{u}}, \text{div} \mathbf{N} \rangle = 0 \quad (2.17a)$$

$$\langle \dot{\mathbf{u}}, \ddot{\mathbf{u}} \rangle + \langle \nabla \dot{\mathbf{u}}, \mathbf{N} \rangle \stackrel{(2.10)}{=} 0 \quad (2.17b)$$

$$\langle \dot{\mathbf{u}}, \ddot{\mathbf{u}} \rangle + \langle \frac{1}{2} (\nabla \dot{\mathbf{u}} + \nabla \dot{\mathbf{u}}^T), \mathbf{N} \rangle \stackrel{(2.12)}{=} 0 \quad (2.17c)$$

$$\frac{d}{dt} \mathcal{T}_m + \langle \frac{1}{2} (\nabla \dot{\mathbf{u}} + \nabla \dot{\mathbf{u}}^T), \mathbf{N} \rangle \stackrel{(2.8)}{=} 0 \quad (2.17d)$$

where the in-plane kinetic energy  $\mathcal{T}_m$  is defined as

$$\mathcal{T}_m = \frac{1}{2} \|\dot{\mathbf{u}}\|^2 \geq 0 \quad (2.18)$$

Similarly, taking the scalar inner product of (2.1b) with  $\dot{w}$  gives

$$\langle \dot{w}, \ddot{w} \rangle - \langle \dot{w}, \text{div} \text{div} \mathbf{M} \rangle - \langle \dot{w}, \text{div} (\mathbf{N} \nabla w) \rangle = 0 \quad (2.19a)$$

$$\langle \dot{w}, \ddot{w} \rangle - \langle \nabla \nabla \dot{w}, \mathbf{M} \rangle + \langle \nabla \dot{w}, \mathbf{N} \nabla w \rangle \stackrel{(2.10)}{=} 0 \quad (2.19b)$$

$$\langle \dot{w}, \ddot{w} \rangle - \langle \nabla \nabla \dot{w}, \mathbf{M} \rangle + \langle \frac{1}{2} (\nabla \dot{w} \otimes \nabla w + \nabla w \otimes \nabla \dot{w}), \mathbf{N} \rangle \stackrel{(2.11)(2.12)}{=} 0 \quad (2.19c)$$

$$\frac{d}{dt} \mathcal{T}_b + \langle \nabla \nabla \dot{w}, \phi(\nabla \nabla w) \rangle + \langle \frac{1}{2} (\nabla \dot{w} \otimes \nabla w + \nabla w \otimes \nabla \dot{w}), \mathbf{N} \rangle \stackrel{(2.8)(2.1c)}{=} 0 \quad (2.19d)$$

where, using (2.9), the bending kinetic energy  $\mathcal{T}_b$  is defined as

$$\mathcal{T}_b = \frac{1}{2} \|\dot{w}\|^2 \geq 0 \quad (2.20)$$

Adding (2.17d) and (2.19d) gives

$$\frac{d}{dt} (\mathcal{T}_m + \mathcal{T}_b) + \langle \nabla \nabla \dot{w}, \phi(\nabla \nabla w) \rangle + \langle \dot{\epsilon}, \phi(\epsilon) \rangle \stackrel{(2.1d)}{=} 0 \quad (2.21)$$

Using identity (2.16), an energy balance results, i.e.,

$$\frac{d}{dt}\mathcal{H} = 0 \quad (2.22)$$

where the Hamiltonian or total energy  $\mathcal{H}$  is defined as

$$\mathcal{H} = \mathcal{T}_m + \mathcal{T}_b + \mathcal{V}_b + \mathcal{V}_m \quad (2.23)$$

where the in-plane potential energy  $\mathcal{V}_m$  and bending potential energy  $\mathcal{V}_b$  are defined as

$$\mathcal{V}_m = \frac{1}{2}\langle \boldsymbol{\epsilon}, \phi(\boldsymbol{\epsilon}) \rangle \quad \mathcal{V}_b = \frac{1}{2}\langle \nabla \nabla w, \phi(\nabla \nabla w) \rangle \quad (2.24)$$

From (2.14), it follows that

$$\mathcal{H} \geq 0 \quad \longrightarrow \quad \mathcal{H}(t) = \mathcal{H}(0) \geq 0 \quad \text{for} \quad t \geq 0 \quad (2.25)$$

### III. SEMI DISCRETE APPROXIMATIONS

In this section, a semi-discrete (in time) approximation to the full von Kármán system (2.1) is introduced, so as to show Hamiltonian construction techniques, regardless of the form of spatial discretization. In particular, care must be taken to split the nonlinear terms, as shown below.

Suppose that the problem is discretized in time, so that functions  $w^n = w^n(x, y)$ ,  $\mathbf{u}^n = \mathbf{u}^n(x, y)$ , are to be calculated at integer time step  $n$ . If the time step is  $k$ , then such functions are approximations to the solution at times  $t = nk$ . All inner product and norm definitions and spatial differentiation identities hold as in the continuous case.

#### A. Time difference and Averaging Operators

For a scalar, vector or tensor  $f = f^n$ , the following shift operators and the identity may be defined as

$$e_{t+}f^n = f^{n+1} \quad e_{t-}f^n = f^{n-1} \quad 1f^n = f^n \quad (3.1)$$

Forward, backward and centered difference operators, all approximations to a first time derivative may be defined in terms of unit shifts and the identity as

$$\delta_{t+} = \frac{1}{k}(e_{t+} - 1) \quad \delta_{t-} = \frac{1}{k}(1 - e_{t-}) \quad \delta_{t\cdot} = \frac{1}{2k}(e_{t+} - e_{t-}) \quad (3.2)$$

A centered approximation to a second time derivative may be defined as

$$\delta_{tt} = \delta_{t+}\delta_{t-} = \frac{1}{k^2}(e_{t+} - 2 + e_{t-}) \quad (3.3)$$

Averaging operators may be defined as

$$\mu_{t+} = \frac{1}{2}(e_{t+} + 1) \quad \mu_{t-} = \frac{1}{2}(1 + e_{t-}) \quad \mu_{t\cdot} = \frac{1}{2}(e_{t+} + e_{t-}) \quad \mu_{tt} = \mu_{t+}\mu_{t-} \quad (3.4)$$

### B. Identities

The following identities hold, for any  $f = f^n$

$$\langle \delta_t f, \delta_{tt} f \rangle = \delta_{t+} \frac{1}{2} \|\delta_{t-} f\|^2 \quad (3.5a)$$

$$\langle \delta_t f, f \rangle = \delta_{t+} \frac{1}{2} \langle f, e_{t-} f \rangle \quad (3.5b)$$

Concerning the mapping  $\phi$ , the following identities hold, for tensors  $\mathbf{F}$  and  $\mathbf{G}$ :

$$\langle \delta_t \mathbf{F}, \phi(\mathbf{F}) \rangle = \delta_{t+} \frac{1}{2} \langle \mathbf{F}, e_{t-} \phi(\mathbf{F}) \rangle \quad (3.6a)$$

$$\delta_{t+} \langle \mathbf{F}, \phi(\mathbf{G}) \rangle = \langle \delta_{t+} \mathbf{F}, \mu_{t+} \phi(\mathbf{G}) \rangle + \langle \mu_{t+} \mathbf{F}, \delta_{t+} \phi(\mathbf{G}) \rangle \quad (3.6b)$$

$$\langle \mathbf{F}, \phi(e_{t-} \mathbf{F}) \rangle = \langle \mu_{t-} \mathbf{F}, \phi(\mu_{t-} \mathbf{F}) \rangle - \frac{k^2}{4} \langle \delta_{t-} \mathbf{F}, \phi(\delta_{t-} \mathbf{F}) \rangle \quad (3.6c)$$

### C. Splitting the Tensor $\mathbf{N}$

The membrane strain tensor  $\boldsymbol{\epsilon}$ , now also semi-discrete in time, with  $\boldsymbol{\epsilon} = \boldsymbol{\epsilon}^n$ , can be decomposed classically as

$$\boldsymbol{\epsilon} = \boldsymbol{\omega} + \boldsymbol{\gamma} \quad \text{with} \quad \boldsymbol{\omega} = \frac{1}{2} (\boldsymbol{\nabla} \mathbf{u} + \boldsymbol{\nabla} \mathbf{u}^T) \quad \boldsymbol{\gamma} = \frac{1}{2} \boldsymbol{\nabla} w \otimes \boldsymbol{\nabla} w \quad (3.7)$$

where  $\boldsymbol{\omega}$  and  $\boldsymbol{\gamma}$  denote respectively the linear and the quadratic part of the strain tensor. Note that  $\boldsymbol{\omega}$  is proportional to the in-plane displacement vector  $\mathbf{u}$  only, whereas the quadratic part involves the transverse displacement  $w$  only.

Accordingly, the in-plane force tensor  $\mathbf{N}$  can be decomposed as:

$$\mathbf{N} = \mathbf{N}_{\mathbf{u}} + \mathbf{N}_w \quad (3.8)$$

where  $\mathbf{N}_{\mathbf{u}}$  groups the linear terms in the in-plane displacement and  $\mathbf{N}_w$  the quadratic terms in  $w$ .

Analyzing the linear and nonlinear terms appearing in the full von Kármán model, one can note the following features:

- Transverse and in-plane motions are linearly decoupled, and nonlinearly coupled.
- The nonlinear coupling for the in-plane motions is quadratic and only due to the term  $\text{div } \mathbf{N}_w$ . Hence in-plane motions are proportional to quadratic terms in the transverse displacement only, formally of the form  $w^2$ .
- For the transverse motions the nonlinear coupling terms involve a quadratic coupling of the form  $\mathbf{u}w$  (coming from the term  $\text{div}(\mathbf{N}_{\mathbf{u}} \boldsymbol{\nabla} w)$ ), and a cubic term of the form  $w^3$  (provided by the term  $\text{div}(\mathbf{N}_w \boldsymbol{\nabla} w)$ ).

### D. Parameterized Approximations and Identities

For a scalar  $w(x, y, t)$ , a three-level symmetric discrete approximation  $w_{\xi}^n$  to  $w(x, y, t)$  at  $t = nk$ , parameterized by the real number  $\xi$  is

$$w_{\xi}^n = \xi w^n + (1 - \xi) \mu_{t-} w^n \quad (3.9)$$

For the quantity  $\boldsymbol{\gamma} = \frac{1}{2} (\boldsymbol{\nabla} w \otimes \boldsymbol{\nabla} w)$ , a parameterized approximation, again over three time levels, is

$$\boldsymbol{\gamma}_{\xi} = \frac{\xi}{4} (\mu_{t-} \boldsymbol{\nabla} w \otimes \boldsymbol{\nabla} w + \boldsymbol{\nabla} w \otimes \mu_{t-} \boldsymbol{\nabla} w) + \frac{1 - \xi}{2} \mu_{tt} (\boldsymbol{\nabla} w \otimes \boldsymbol{\nabla} w) \quad (3.10)$$

A parameterized (backwards) approximation over two time levels is

$$\gamma_{\xi-} = \frac{\xi}{4} (e_{t-} \nabla w \otimes \nabla w + \nabla w \otimes e_{t-} \nabla w) + \frac{1-\xi}{2} \mu_{t-} (\nabla w \otimes \nabla w) \quad (3.11)$$

The following identities hold:

$$\gamma_{\xi-} = \mu_{t+} \gamma_{\xi-} \quad (3.12a)$$

$$\delta_{t+} \gamma_{\xi-} = \frac{1}{2} (\delta_t \nabla w \otimes \nabla w_{\xi} + \nabla w_{\xi} \otimes \delta_t \nabla w) \quad (3.12b)$$

A backwards approximation to  $\omega$  is given by

$$\omega_- = \mu_{t-} \omega \quad (3.13)$$

#### E. Semi-discrete Schemes for the von Kármán System

Consider two step schemes of the following form, which follow from (2.1a) and (2.1b):

$$\delta_{tt} \mathbf{u} - \operatorname{div} (\hat{\mathbf{N}}_{\mathbf{u}} + \hat{\mathbf{N}}_w) = 0 \quad (3.14a)$$

$$\delta_{tt} w - \operatorname{div} \operatorname{div} \mathbf{M} - \operatorname{div} (\bar{\mathbf{N}}_{\mathbf{u}} \nabla \tilde{w} + \bar{\mathbf{N}}_w \nabla \tilde{w}) = 0 \quad (3.14b)$$

Here,  $\hat{\mathbf{N}}_{\mathbf{u}} = \hat{\mathbf{N}}_{\mathbf{u}}^n$  and  $\bar{\mathbf{N}}_{\mathbf{u}} = \bar{\mathbf{N}}_{\mathbf{u}}^n$  represent approximations (possibly distinct) to  $\mathbf{N}_{\mathbf{u}}$  at  $t = nk$ , and similarly,  $\hat{\mathbf{N}}_w = \hat{\mathbf{N}}_w^n$  and  $\bar{\mathbf{N}}_w = \bar{\mathbf{N}}_w^n$  approximations (possibly distinct) to  $\mathbf{N}_w$  at  $t = nk$ .  $\tilde{w} = \tilde{w}^n$  and  $\tilde{\tilde{w}} = \tilde{\tilde{w}}^n$  are approximations to  $w$ , again at  $t = nk$ . The forms of these approximations will be specified subsequently.  $\mathbf{M} = \mathbf{M}^n$  is defined as in (2.1c).

Similarly to the fully continuous case, one may take inner products of (3.14a) and (3.14b) with  $\delta_t \mathbf{u}$  and  $\delta_t w$  to get

$$\langle \delta_t \mathbf{u}, \delta_{tt} \mathbf{u} \rangle - \langle \delta_t \mathbf{u}, \operatorname{div} (\hat{\mathbf{N}}_{\mathbf{u}} + \hat{\mathbf{N}}_w) \rangle = 0 \quad (3.15a)$$

$$\langle \delta_t w, \delta_{tt} w \rangle - \langle \delta_t w, \operatorname{div} \operatorname{div} \mathbf{M} \rangle - \langle \delta_t w, \operatorname{div} (\bar{\mathbf{N}}_{\mathbf{u}} \nabla \tilde{w} + \bar{\mathbf{N}}_w \nabla \tilde{w}) \rangle = 0 \quad (3.15b)$$

Using identities (3.5a) and (3.5b), and integration by parts for the second term in (3.15b), and adding the two equations, one may arrive at

$$\delta_{t+} (\mathcal{T}_m + \mathcal{T}_b + \mathcal{V}_b) - \langle \delta_t \mathbf{u}, \operatorname{div} (\hat{\mathbf{N}}_{\mathbf{u}} + \hat{\mathbf{N}}_w) \rangle - \langle \delta_t w, \operatorname{div} (\bar{\mathbf{N}}_{\mathbf{u}} \nabla \tilde{w} + \bar{\mathbf{N}}_w \nabla \tilde{w}) \rangle = 0 \quad (3.16)$$

where

$$\mathcal{T}_m = \frac{1}{2} \|\delta_{t-} \mathbf{u}\|^2 \quad \mathcal{T}_b = \frac{1}{2} \|\delta_{t-} w\|^2 \quad \mathcal{V}_b = \frac{1}{2} \langle \nabla \nabla w, e_{t-} \phi(\nabla \nabla w) \rangle \quad (3.17)$$

Furthermore, using integration by parts (2.10), one may continue to

$$\delta_{t+} (\mathcal{T}_m + \mathcal{T}_b + \mathcal{V}_b) + \langle \delta_t \nabla \mathbf{u}, \hat{\mathbf{N}}_{\mathbf{u}} + \hat{\mathbf{N}}_w \rangle + \langle \delta_t \nabla w, \bar{\mathbf{N}}_{\mathbf{u}} \nabla \tilde{w} + \bar{\mathbf{N}}_w \nabla \tilde{w} \rangle = 0 \quad (3.18)$$

Restricting  $\hat{\mathbf{N}}_{\mathbf{u}}$ ,  $\hat{\mathbf{N}}_w$ ,  $\bar{\mathbf{N}}_{\mathbf{u}}$  and  $\bar{\mathbf{N}}_w$  to be symmetric (as is the case for  $\mathbf{N}$  itself), one may go further, using identities (2.11) and (2.12), and definition (3.7), to

$$\begin{aligned} \delta_{t+} (\mathcal{T}_m + \mathcal{T}_b + \mathcal{V}_b) + \langle \delta_t \boldsymbol{\omega}, \hat{\mathbf{N}}_{\mathbf{u}} + \hat{\mathbf{N}}_w \rangle + \frac{1}{2} \langle \delta_t \nabla w \otimes \nabla \tilde{w} + \nabla \tilde{w} \otimes \delta_t \nabla w, \bar{\mathbf{N}}_{\mathbf{u}} \rangle & (3.19) \\ + \frac{1}{2} \langle \delta_t \nabla w \otimes \nabla \tilde{w} + \nabla \tilde{w} \otimes \delta_t \nabla w, \bar{\mathbf{N}}_w \rangle & = 0 \end{aligned}$$

At this point definitions of the approximations  $\hat{\mathbf{N}}_{\mathbf{u}}$ ,  $\bar{\mathbf{N}}_{\mathbf{u}}$ ,  $\hat{\mathbf{N}}_w$ ,  $\bar{\mathbf{N}}_w$ ,  $\tilde{w}$  and  $\tilde{\tilde{w}}$  are necessary. The goal is to find such choices such the remaining terms in the energy balance above coalesce into a single time difference of a scalar quantity,  $\mathcal{V}_m$ .

#### F. A Conservative Family of Schemes

There are three sets of terms in (3.19) which need to be examined separately:

- $\langle \delta_t \boldsymbol{\omega}, \hat{\mathbf{N}}_{\mathbf{u}} \rangle$
- $\langle \delta_t \boldsymbol{\omega}, \hat{\mathbf{N}}_w \rangle + \frac{1}{2} \langle \delta_t \boldsymbol{\nabla} w \otimes \boldsymbol{\nabla} \tilde{w} + \boldsymbol{\nabla} \tilde{w} \otimes \delta_t \boldsymbol{\nabla} w, \bar{\mathbf{N}}_{\mathbf{u}} \rangle$
- $\frac{1}{2} \langle \delta_t \boldsymbol{\nabla} w \otimes \boldsymbol{\nabla} \tilde{\tilde{w}} + \boldsymbol{\nabla} \tilde{\tilde{w}} \otimes \delta_t \boldsymbol{\nabla} w, \bar{\mathbf{N}}_w \rangle$

Consider the following choices of approximation:

$$\hat{\mathbf{N}}_{\mathbf{u}} = \phi(\boldsymbol{\omega}) \quad (3.20a)$$

$$\bar{\mathbf{N}}_{\mathbf{u}} = \mu_{tt} \phi(\boldsymbol{\omega}) \quad (3.20b)$$

$$\tilde{\tilde{w}} = w_\alpha \quad (3.20c)$$

$$\tilde{w} = w_\beta \quad (3.20d)$$

$$\bar{\mathbf{N}}_w = \phi(\boldsymbol{\gamma}_{\alpha \cdot}) \quad (3.20e)$$

$$\hat{\mathbf{N}}_w = \phi(\boldsymbol{\gamma}_{\beta \cdot}) \quad (3.20f)$$

The latter four approximations are parameterized by the real numbers  $\alpha$  and  $\beta$ , as per the discussion in Section III D.

Concerning the first term above, and using the definition (3.20a) and identity (3.6a):

$$\langle \delta_t \boldsymbol{\omega}, \hat{\mathbf{N}}_{\mathbf{u}} \rangle = \langle \delta_t \boldsymbol{\omega}, \phi(\boldsymbol{\omega}) \rangle = \delta_{t+} \frac{1}{2} \langle \boldsymbol{\omega}, e_{t-} \phi(\boldsymbol{\omega}) \rangle \quad (3.21)$$

Concerning the second term above, using definitions (3.20b), (3.20d) and (3.20f), as well as identity (3.12b), it may be rewritten as

$$\langle \delta_t \boldsymbol{\omega}, \hat{\mathbf{N}}_w \rangle + \frac{1}{2} \langle \delta_t \boldsymbol{\nabla} w \otimes \boldsymbol{\nabla} \tilde{w} + \boldsymbol{\nabla} \tilde{w} \otimes \delta_t \boldsymbol{\nabla} w, \bar{\mathbf{N}}_{\mathbf{u}} \rangle = \langle \delta_t \boldsymbol{\omega}, \phi(\boldsymbol{\gamma}_{\beta \cdot}) \rangle + \langle \delta_{t+} \boldsymbol{\gamma}_{\beta -}, \mu_{tt} \phi(\boldsymbol{\omega}) \rangle \quad (3.22)$$

or, using definition (3.13) and identity (3.12a), as

$$\langle \delta_{t+} \boldsymbol{\omega}_-, \mu_{t+} \phi(\boldsymbol{\gamma}_{\beta -}) \rangle + \langle \delta_{t+} \boldsymbol{\gamma}_{\beta -}, \mu_{t+} \phi(\boldsymbol{\omega}_-) \rangle \quad (3.23)$$

Finally, using identity (3.6b), this may be rewritten as

$$\langle \delta_{t+} \boldsymbol{\omega}_-, \mu_{t+} \phi(\boldsymbol{\gamma}_{\beta -}) \rangle + \langle \mu_{t+} \boldsymbol{\omega}_-, \delta_{t+} \phi(\boldsymbol{\gamma}_{\beta -}) \rangle = \delta_{t+} \langle \boldsymbol{\omega}_-, \phi(\boldsymbol{\gamma}_{\beta -}) \rangle \quad (3.24)$$

The third term may be written, using the definitions (3.20e) and (3.20c), and identity (3.6b), as

$$\langle \delta_{t+} \boldsymbol{\gamma}_{\alpha -}, \phi(\boldsymbol{\gamma}_{\alpha \cdot}) \rangle = \langle \delta_{t+} \boldsymbol{\gamma}_{\alpha -}, \mu_{t+} \phi(\boldsymbol{\gamma}_{\alpha -}) \rangle = \delta_{t+} \frac{1}{2} \langle \boldsymbol{\gamma}_{\alpha -}, \phi(\boldsymbol{\gamma}_{\alpha -}) \rangle \quad (3.25)$$

This family of schemes, dependent on the parameters  $\alpha$  and  $\beta$ , is thus conservative:

$$\delta_{t+} \mathcal{H} = 0 \quad \mathcal{H} = \mathcal{T}_m + \mathcal{T}_b + \mathcal{V}_b + \mathcal{V}_m \quad (3.26)$$

where  $\mathcal{V}_m$  given by

$$\mathcal{V}_m = \frac{1}{2} \langle \boldsymbol{\omega}, e_{t-} \phi(\boldsymbol{\omega}) \rangle + \langle \boldsymbol{\omega}_-, \phi(\boldsymbol{\gamma}_{\beta-}) \rangle + \frac{1}{2} \langle \boldsymbol{\gamma}_{\alpha-}, \phi(\boldsymbol{\gamma}_{\alpha-}) \rangle \quad (3.27)$$

A further manipulation leads to great simplification in subsequent analysis. The expressions for  $\mathcal{V}_m$  in (3.17) and the first term in  $\mathcal{V}_m$  in (3.27) above may be written, using identity (3.6c) as

$$\begin{aligned} \frac{1}{2} \langle \boldsymbol{\omega}, e_{t-} \phi(\boldsymbol{\omega}) \rangle &= \frac{1}{2} \langle \boldsymbol{\omega}_-, \phi(\boldsymbol{\omega}_-) \rangle - \frac{k^2}{8} \langle \delta_{t-} \boldsymbol{\omega}, \phi(\delta_{t-} \boldsymbol{\omega}) \rangle \\ \frac{1}{2} \langle \nabla \nabla w, e_{t-} \phi(\nabla \nabla w) \rangle &= \frac{1}{2} \langle \mu_{t-}, \nabla \nabla w, \mu_{t-} \phi(\nabla \nabla w) \rangle - \frac{k^2}{8} \langle \delta_{t-} \nabla \nabla w, \delta_{t-} \phi(\nabla \nabla w) \rangle \end{aligned} \quad (3.28)$$

The conserved energy  $\mathcal{H}$  may then be rewritten as

$$\mathcal{H} = \mathcal{T}'_m + \mathcal{T}'_b + \mathcal{V}'_b + \mathcal{V}'_m \quad (3.29)$$

where

$$\mathcal{T}'_m = \frac{1}{2} \|\delta_{t-} \mathbf{u}\|^2 - \frac{k^2}{8} \langle \delta_{t-} \boldsymbol{\omega}, \phi(\delta_{t-} \boldsymbol{\omega}) \rangle \quad (3.30a)$$

$$\mathcal{T}'_b = \frac{1}{2} \|\delta_{t-} w\|^2 - \frac{k^2}{8} \langle \delta_{t-} \nabla \nabla w, \delta_{t-} \phi(\nabla \nabla w) \rangle \quad (3.30b)$$

$$\mathcal{V}'_b = \frac{1}{2} \langle \mu_{t-}, \nabla \nabla w, \mu_{t-} \phi(\nabla \nabla w) \rangle \quad (3.30c)$$

$$\mathcal{V}'_m = \frac{1}{2} \langle \boldsymbol{\omega}_-, \phi(\boldsymbol{\omega}_-) \rangle + \langle \boldsymbol{\omega}_-, \phi(\boldsymbol{\gamma}_{\beta-}) \rangle + \frac{1}{2} \langle \boldsymbol{\gamma}_{\alpha-}, \phi(\boldsymbol{\gamma}_{\alpha-}) \rangle \quad (3.30d)$$

In this form, it is particularly simple to arrive at bounds on solution size in the fully discrete case. See Section IV D.

#### G. Special Case: $\alpha = \beta$

When  $\alpha = \beta$ , the energy term  $\mathcal{V}'_m$  may be simplified to

$$\mathcal{V}'_m = \frac{1}{2} \langle \boldsymbol{\omega}_- + \boldsymbol{\gamma}_{\alpha-}, \phi(\boldsymbol{\omega}_- + \boldsymbol{\gamma}_{\alpha-}) \rangle = \frac{1}{2} \langle \boldsymbol{\epsilon}_{\alpha-}, \phi(\boldsymbol{\epsilon}_{\alpha-}) \rangle \geq 0 \quad \text{where} \quad \boldsymbol{\epsilon}_{\alpha-} = \boldsymbol{\omega}_- + \boldsymbol{\gamma}_{\alpha-} \quad (3.31)$$

Here, contributions to the total energy due to nonlinear effects are assured to be non-negative (note also that  $\mathcal{V}'_m \geq 0$ ), leading to great simplification in the subsequent analysis of stability in fully discrete schemes. In essence, stability analysis reduces to the analysis of the linear problem—i.e., determining conditions for non-negativity of the kinetic energy terms  $\mathcal{T}'_m$  and  $\mathcal{T}'_b$ .

There are more general conditions on the parameters  $\alpha$  and  $\beta$  such that  $\mathcal{V}'_m \geq 0$ , but given the practical importance of the case  $\alpha = \beta = 1$  (see below), such conditions will not be explored further here.

#### H. Special Case: $\alpha = \beta = 1$

The scheme (3.14) is necessarily implicit. When either  $\alpha \neq 1$  or  $\beta \neq 1$ , however, at a given time step, the determination of unknown values in terms of previously computed values requires the solution of nonlinear equations, leading to new concerns regarding existence and uniqueness.

When  $\alpha = \beta = 1$ , however, the unknowns appear linearly, and thus may be solved for uniquely. Expanding the various time difference and averaging operators in (3.14) explicitly at time step  $n$  leads to update equations of the form

$$\mathbf{A}(\mathbf{u}^n, w^n) \begin{bmatrix} \mathbf{u}^{n+1} \\ w^{n+1} \end{bmatrix} = \mathbf{b}(\mathbf{u}^n, w^n, \mathbf{u}^{n-1}, w^{n-1}) \quad (3.32)$$

Here,  $[\mathbf{u}^{n+1}, w^{n+1}]^T$  represents the unknown state at the next time step ( $n+1$ ), and the operators  $\mathbf{A}$  and  $\mathbf{b}$  depend only on previously computed values at the time steps  $n$  and  $n-1$ . In particular, in the fully discrete case, the operator  $\mathbf{A}$  may be written as a square matrix dependent on previously computed values, and a linear system solution will be required for the update.

#### IV. FULLY DISCRETE SCHEMES

The family of schemes described in the previous section is semi-discrete in time, and possesses an energy conservation property. Spatial discretization is as yet unspecified, and may be carried out in a variety of ways—finite element methods are often used, but pseudospectral methods have also been employed for a variant of this system [40, 33].

For illustrative purposes, in this section, a simple discretization over a regular grid will be employed. The grid functions  $w$  and  $\mathbf{u}$ ,

$$w_{l,m}^n \quad \mathbf{u}_{l,m}^n \quad (l, m) \in \Omega_Q = \{(l, m) | 0 \leq l, m \leq Q-1\} \quad (4.1)$$

are approximations to  $w^n(x, y)$  and  $\mathbf{u}^n(x, y)$  at  $x = lh$  and  $y = mh$  over the periodic domain  $\Omega_Q$  corresponding to a square of side length  $L$ , where  $h$ , the grid spacing is defined as  $h = L/Q$  for some positive integer  $Q$ .

##### A. Inner Products, Difference and Fourier Operators and Summation by Parts

For any two grid functions  $\mathbf{F}_{l,m}$  and  $\mathbf{G}_{l,m}$  (again scalars, vectors, or general rectangular matrices), the  $l^2$  spatial inner product and norm over  $\Omega_Q$  are defined as

$$\langle \mathbf{F}, \mathbf{G} \rangle = h^2 \sum_{(l,m) \in \Omega_Q} \mathbf{F}_{l,m} \diamond \mathbf{G}_{l,m} \quad \|\mathbf{F}\| = \langle \mathbf{F}, \mathbf{F} \rangle^{1/2} \quad (4.2)$$

where the  $\diamond$  operation is as defined in (2.6). Consider now a generic difference operator  $\mathbf{D} = [\mathbf{D}_x \mathbf{D}_y]$  approximating the gradient  $\nabla$  over the grid  $\Omega_Q$ . Similarly to the case of integration by parts, such an operator will satisfy a summation by parts identity with an associated operator,  $\mathbf{D}^\dagger$ , representing an approximation to the divergence operation:

$$\langle f, \mathbf{D}^\dagger \mathbf{g} \rangle = -\langle \mathbf{D}f, \mathbf{g} \rangle \quad (4.3)$$

There are obviously many choices of such an operator; the simplest possible choices are  $\mathbf{D} = \mathbf{D}_+ = [\mathbf{D}_{x+} \mathbf{D}_{y+}]^T$  and  $\mathbf{D} = \mathbf{D}_- = [\mathbf{D}_{x-} \mathbf{D}_{y-}]^T$ , representing forward and backward difference operations. In terms of (say) a vector grid function  $\mathbf{f}_{l,m}^n$ , the operations  $\mathbf{D}_{x+}$  and  $\mathbf{D}_{x-}$  are defined as:

$$\mathbf{D}_{x+} \mathbf{f}_{l,m}^n = \frac{1}{h} (\mathbf{f}_{l+1,m}^n - \mathbf{f}_{l,m}^n) \quad \mathbf{D}_{x-} \mathbf{f}_{l,m}^n = \frac{1}{h} (\mathbf{f}_{l,m}^n - \mathbf{f}_{l-1,m}^n) \quad (4.4)$$

where spatial indices  $l$  are taken modulo  $Q$ . A similar definition holds for  $\mathbf{D}_{y+}$  and  $\mathbf{D}_{y-}$ . The associated divergence operations are  $\mathbf{D}_+^\dagger = \mathbf{D}_-^T$  and  $\mathbf{D}_-^\dagger = \mathbf{D}_+^T$ .

Another useful choice of approximation (used often in studies of wave turbulence) is the Fourier spectral gradient  $\mathbf{D} = \mathbf{D}_{spec} = [\mathbf{D}_{spec,x} \mathbf{D}_{spec,y}]^T$ . When applied, e.g., to a vector function  $\mathbf{f}_{l,m}^n$ , the operator  $\mathbf{D}_{spec,x}$  may be written as

$$(\mathbf{D}_{spec,x} \mathbf{f})_{l,m}^n = \pi \sum_{l'=0, l' \neq l}^{N-1} (-1)^{l-l'} \cot\left(\frac{\pi(l-l')}{Q}\right) \mathbf{f}_{l,m}^n \quad (4.5)$$

with a similar definition holding for  $\mathbf{D}_{spec,y}$ . Such operators may be efficiently applied using the Fast Fourier Transform [51].

### B. Operator Bounds

For a given difference approximation acting over a grid function defined over  $\Omega_Q$ , it is assumed here that the operation is bounded. For a gradient approximation  $\mathbf{D}$  applied to a vector or scalar grid function  $\mathbf{f}_{l,m}^n$ , for instance, one has

$$\|\mathbf{D}\mathbf{f}\| \leq D_{max} \|\mathbf{f}\| \quad \text{and} \quad \left\| \frac{1}{2} (\mathbf{D}\mathbf{f} + (\mathbf{D}\mathbf{f})^T) \right\| \leq D_{max} \|\mathbf{f}\| \quad (4.6)$$

For the simple forward and backward difference operations  $\mathbf{D}_+$  and  $\mathbf{D}_-$ , for example, one has  $D_{\pm, max} = 2\sqrt{2}/h$ . For the spectral operator  $\mathbf{D}_{spec}$ , the bound exhibits a slightly more complex dependence on  $h$ , but in the limit of small time steps, one has approximately  $D_{spec, max} = \sqrt{2}\pi/h$ . The associated divergence operators  $\mathbf{D}^\dagger$  are subject to the same bound, i.e.,  $D_{max}^\dagger = D_{max}$ .

### C. Discrete Method and Conserved Energy

One may proceed directly from the semi-discrete system (3.14) to a fully discrete method

$$\delta_{tt} \mathbf{u} - \mathbf{D}_a^\dagger (\hat{\mathbf{N}}_{\mathbf{u}} + \hat{\mathbf{N}}_w) = 0 \quad (4.7a)$$

$$\delta_{tt} w - \mathbf{D}_b^\dagger \mathbf{D}_c^\dagger \mathbf{M} - \mathbf{D}_a^\dagger (\bar{\mathbf{N}}_{\mathbf{u}} \mathbf{D}_a \tilde{w} + \bar{\mathbf{N}}_w \mathbf{D}_a \tilde{\tilde{w}}) = 0 \quad (4.7b)$$

where here, all variables are assumed defined over  $\Omega_Q$ , and where the various approximations to the gradient operation  $\mathbf{D}_a$ ,  $\mathbf{D}_b$  and  $\mathbf{D}_c$  (possibly distinct) have been employed.

$\mathbf{M}$  is approximated as

$$\mathbf{M} = -\phi(\mathbf{D}_c \mathbf{D}_b w) \quad (4.8)$$

and the tensors  $\hat{\mathbf{N}}_{\mathbf{u}}$ ,  $\hat{\mathbf{N}}_w$ ,  $\bar{\mathbf{N}}_{\mathbf{u}}$  and  $\bar{\mathbf{N}}_w$  and the grid functions  $\tilde{w}$  and  $\tilde{\tilde{w}}$  as in (3.20). The quantity  $\omega$  is as defined in (3.7), and  $\gamma_{\xi-}$  and  $\gamma_{\xi-}$  are as defined in (3.10) and (3.11), with the operator  $\mathbf{D}_a$  replacing  $\nabla$ .

Consider the scheme (4.7) with  $\alpha = \beta$ . The energy analysis of the semi-discrete case follows through as before, where now, the various components are defined as

$$\mathcal{T}'_m = \frac{1}{2} \|\delta_{t-} \mathbf{u}\|^2 - \frac{k^2}{8} \langle \delta_{t-} \omega, \phi(\delta_{t-} \omega) \rangle \quad (4.9a)$$

$$\mathcal{T}'_b = \frac{1}{2} \|\delta_{t-} w\|^2 - \frac{k^2}{8} \langle \delta_{t-} \mathbf{D}_c \mathbf{D}_b w, \delta_{t-} \phi(\mathbf{D}_c \mathbf{D}_b w) \rangle \quad (4.9b)$$

$$\mathcal{V}'_b = \frac{1}{2} \langle \mu_{t-} \mathbf{D}_c \mathbf{D}_b w, \mu_{t-} \phi(\mathbf{D}_c \mathbf{D}_b w) \rangle \quad (4.9c)$$

$$\mathcal{V}'_m = \frac{1}{2} \langle \epsilon_{\alpha-}, \phi(\epsilon_{\alpha-}) \rangle \quad (4.9d)$$

#### D. Non-negativity Conditions

Note that by (2.14),  $\mathcal{V}'_m \geq 0$ , and  $\mathcal{V}'_b \geq 0$ . What remains is to bound the terms  $\mathcal{T}'_m$  and  $\mathcal{T}'_b$  away from zero. To this end, note that from (2.15), one has

$$\langle \delta_{t-}\boldsymbol{\omega}, \phi(\delta_{t-}\boldsymbol{\omega}) \rangle = \nu \|\text{tr}(\delta_{t-}\boldsymbol{\omega})\|^2 + (1-\nu) \|\delta_{t-}\boldsymbol{\omega}\|^2 \quad (4.10a)$$

$$= \nu \|\mathbf{D}_a^\dagger(\delta_{t-}\mathbf{u})\|^2 + (1-\nu) \|\delta_{t-}\left(\frac{1}{2}\left(\mathbf{D}_a\mathbf{u} + (\mathbf{D}_a\mathbf{u})^T\right)\right)\|^2 \quad (4.10b)$$

$$\leq D_{a,max}^2 \|\delta_{t-}\mathbf{u}\|^2 \quad (4.10c)$$

and

$$\langle \delta_{t-}\mathbf{D}_c\mathbf{D}_b w, \delta_{t-}\phi(\mathbf{D}_c\mathbf{D}_b w) \rangle = \nu \|\text{tr}(\delta_{t-}\mathbf{D}_c\mathbf{D}_b w)\|^2 + (1-\nu) \|\delta_{t-}\mathbf{D}_c\mathbf{D}_b w\|^2 \quad (4.11a)$$

$$\leq D_{c,max}^2 D_{b,max}^2 \|\delta_{t-}w\|^2 \quad (4.11b)$$

Thus under the conditions

$$k \leq \frac{2}{D_{a,max}} \quad k \leq \frac{2}{D_{b,max}D_{c,max}} \quad (4.12)$$

the terms  $\mathcal{T}'_m$  and  $\mathcal{T}'_b$  are non-negative. For simple difference operations, these bounds are equivalent to those arrived at through von Neumann analysis of the linear part of the von Kármán system alone. For example, if  $\mathbf{D}_a = \mathbf{D}_+$ ,  $\mathbf{D}_b = \mathbf{D}_+$  and  $\mathbf{D}_c = \mathbf{D}_-$ , the conditions above reduce to  $k \leq h/\sqrt{2}$  and  $k \leq h^2/4$ , for a grid spacing  $h$ . For the spectral scheme, with  $\mathbf{D}_a = \mathbf{D}_b = \mathbf{D}_c = \mathbf{D}_{spec}$ , then  $k \leq \sqrt{2}h/\pi$  and  $k \leq h^2/\pi^2$ .

#### E. Summary

In sum, the method proposed here in (3.14), defined over a discrete periodic domain is energy conserving, and dependent on two free parameters  $\alpha$  and  $\beta$ . Under the choices  $\alpha = \beta = 1$ , the discrete energy function can be shown to be non-negative under simple conditions on the grid spacing in terms of the time step, as for the underlying linear problem. The property is independent of the particular type of spatial discretization, and both simple finite difference and Fourier based methods have been described here. For readers wishing to examine the implementation of such an algorithm, Matlab code is available as supplementary material. See reference [52] below.

## V. SIMULATION RESULTS

Simple examples of the use of the fully discrete method described above are presented in this section. As a useful test configuration, consider an initialisation, over the periodic square domain  $\Omega_Q$  with the first sinusoidal mode shape in the transverse displacement:

$$w_{i,m}^0 = w_{i,m}^1 = a \cos(2\pi l/Q) \cos(2\pi m/Q) \quad \mathbf{u}_{i,m}^0 = \mathbf{u}_{i,m}^1 = 0 \quad (5.1)$$

where here,  $a$  is a nondimensional amplitude. (Recall that amplitudes have been scaled with respect to the quantity  $H/\sqrt{12}$ , where  $H$  is the physical plate thickness.) The non-dimensional side length  $L$  is chosen as  $L = 20$  in all cases, and Poisson's ratio  $\nu$  is set to  $\nu = 0.3$ .

## A. Time Evolution of Plate Profile under Different Initial Condition Amplitudes

As a first example, consider the use of the scheme (3.14), with  $\alpha = \beta = 1$ , and using a simple finite difference discretization as given in Section IV A, and employing varying initial condition amplitudes  $a$ .

Under very small amplitude conditions (here,  $a = 0.01$ ), the plate undergoes transverse vibration in its first linear mode, at nondimensional frequency  $4\pi/L^2$ . See Figure 1. As the initial amplitude is increased, particularly beyond approximately  $a = 1$ , the gross frequency of vibration of the plate increases, and as  $a$  is increased further, beyond about  $a = 3$ , one begins to see transfer of energy to other modes, and the vibration is in general aperiodic. See Figure 2. See also Figure 3, showing the displacement of the corner value of the displacement  $w_{0,0}^n$  as a function of time, for various different initial condition amplitudes. The time step here is chosen as  $k = 1/50$ , and the simple finite difference discretization described in Section IV A is employed, with  $h$  chosen to satisfy the stability bounds (4.12) as close to equality as possible. In this case, the grid size is given by  $Q = 70$ .

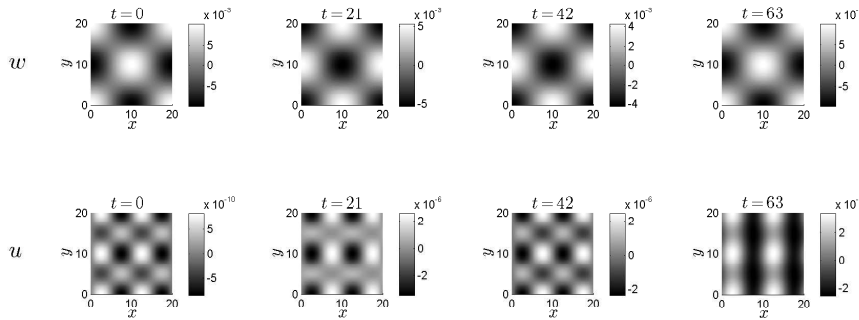


FIG. 1. Snapshots of plate displacement, under an initial condition of the first linear mode shape, with  $a = 0.01$ , at times as indicated. The transverse displacement field  $w$  is shown along the top row, and one longitudinal displacement (the first component of  $\mathbf{u}$ ) on the bottom row. Light and dark indicate regions of positive and negative displacement, respectively.

## B. Fourier vs. Finite Difference Approximations

Particularly at high initial condition amplitudes, calculated solutions using a simple spatial discretization method such as finite differences are subject to substantial drift. See Figure 4, showing a comparison between a high accuracy solution, calculated using a small time step, and one calculated using a coarse spatial grid with a larger time step. As might be expected, the Fourier discretization does a much better job, and solutions calculated using a large time step over a coarse spatial grid match well with those from an accurate finite difference scheme. See Figure 4. Particularly when it is of interest to examine delicate phenomena such as e.g., mode bifurcations under forced conditions, such a method (which is similar to modal methods used previously [11]) will be preferred. Note, however, that in a conservative scheme which can be written in an update form such as (3.32), the difference matrices will no longer be sparse, so that the computational

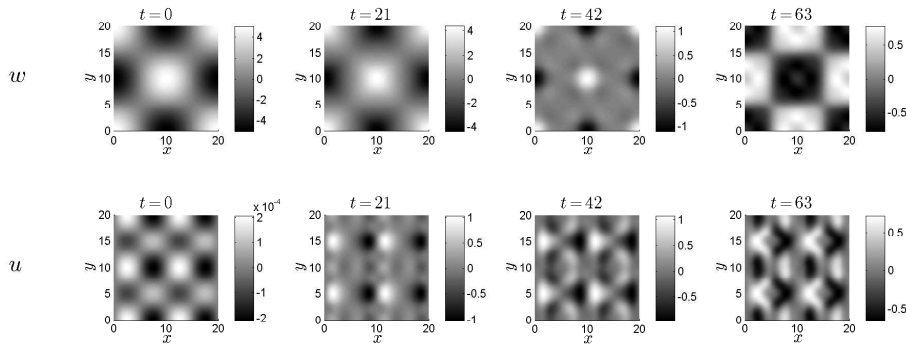


FIG. 2. Snapshots of plate displacement, under an initial condition of the first linear mode shape, with  $a = 5$ , at times as indicated. The transverse displacement field  $w$  is shown along the top row, and one longitudinal displacement (the first component of  $\mathbf{u}$ ) on the bottom row. Light and dark indicate regions of positive and negative displacement, respectively.

effort associated with a time update will be considerably larger than in the case of locally defined difference operators.

### C. Energy Conservation

In this section, the energy conservation property of the schemes presented in Section IV. is demonstrated, for various choices of the initial condition amplitude  $a$ . Calculated values of the total conserved energy  $\mathcal{H}$  are given in Table I, for the case of a finite difference discretization, and in Table II for a Fourier discretization.

In both cases, even at high amplitudes, energy is conserved to many places—in this case, in double precision floating point, near the level of machine accuracy. For more comments on accuracy in finite precision, see Section VI.

Also of interest is the partition of the energy into the various potential and kinetic components as defined in (4.9).

## VI. CONCLUDING REMARKS

This article has explored a family of energy conserving numerical methods for the full von Kármán system, in both semi-discrete and fully discrete forms, and, more generally, with construction techniques for implicit numerical time-stepping methods for nonlinear systems. Though, for simplicity, only the doubly periodic domain has been discussed here, along with relatively simple spatial discretization strategies, it is anticipated that nontrivial boundary conditions and more elaborate discretization methods should fit into the framework described here. There are, however, various issues which remain unresolved.

The two-parameter family of schemes given in (3.14), along with the split-tensor time discretizations given in (3.20) leads to a semi-discrete update with a conserved energy. Under appropriate choices of the spatial discretizations, the conservation of energy then follows through to the fully discrete case. The determination of numerical stability

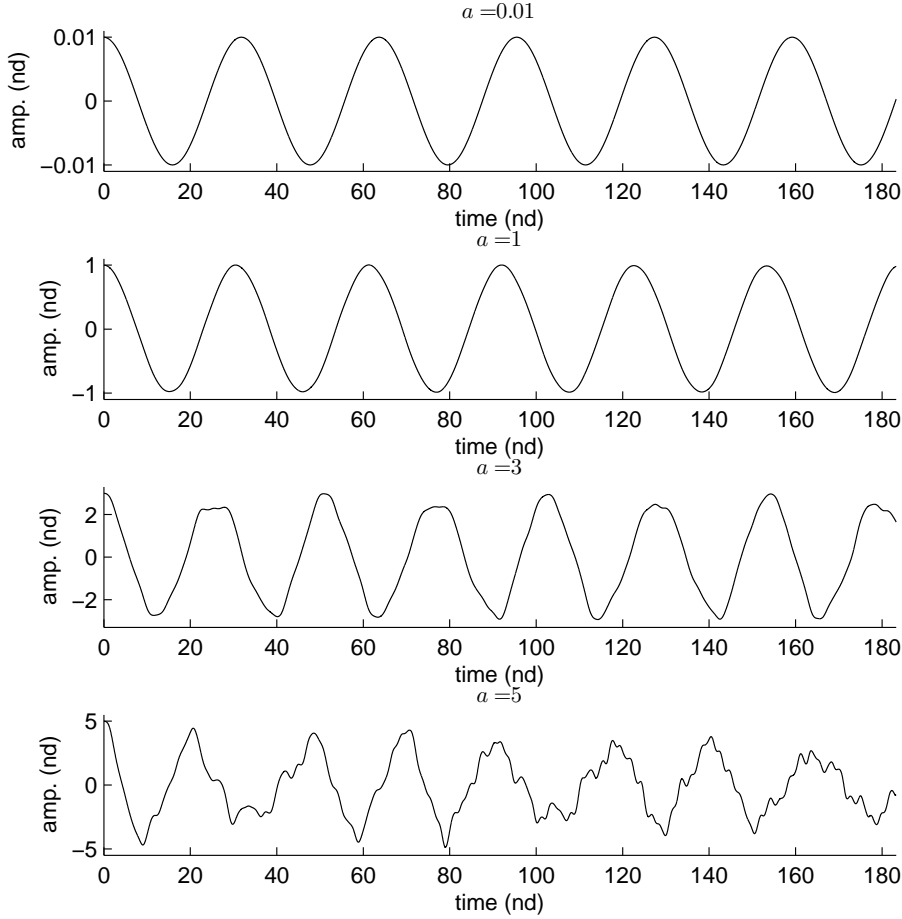


FIG. 3. Plate response, for a plate with  $L = 20$ , and  $\nu = 0.3$ , under an initial condition of the first linear mode shape, for different amplitudes  $a$ , as indicated. The response, taken as  $w_{0,0}^n$ , is plotted against time. The time step is taken as  $k = 1/50$ .

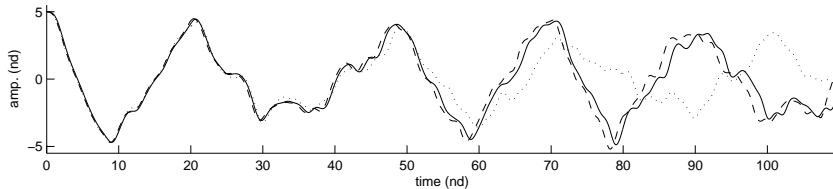


FIG. 4. Plate response, for a plate with  $L = 20$ , and  $\nu = 0.3$ , under an initial condition of the first linear mode shape, for amplitude  $a = 5$ . The response, taken as  $w_{0,0}^n$ , is plotted against time, for three different simulations: Solid line: an accurate response using a finite difference discretization, for  $k = 1/50$ . Dotted line: coarse response using a finite difference discretization, with  $k = 1/10$ . Dashed line: coarse response using a Fourier discretization, with  $k = 1/10$ .

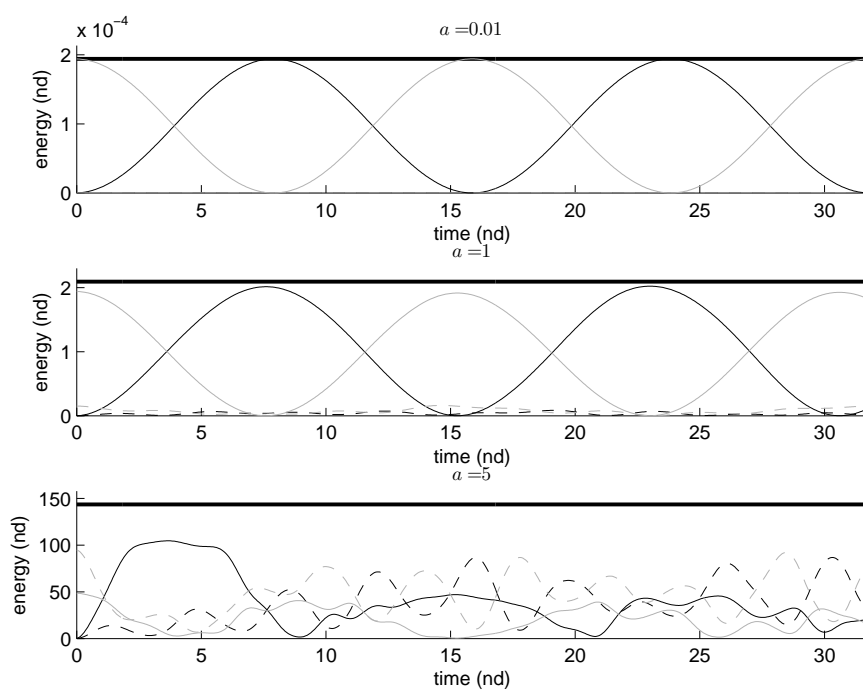


FIG. 5. Partition of numerical energy as a function of time, for a finite difference scheme, under different values of the initial amplitude  $a$ , as indicated. The various components of the energy,  $\mathcal{T}'_b$  (solid black),  $\mathcal{V}'_b$  (solid grey),  $\mathcal{T}'_m$  (dashed black) and  $\mathcal{V}'_m$  (dashed grey), as given in (4.9) are shown. The total energy  $\mathcal{H}$  is indicated by a thick black line. The time step is again  $k = 1/20$ .

reduces to conditions under which the conserved energy is a non-negative function of the state. Under particular choices of the scheme parameters ( $\alpha = \beta$ ), such conditions are easily arrived at, and reduce to stability conditions for the underlying linear system—that is, the additional potential energy associated with the nonlinearity is non-negative. When  $\alpha \neq \beta$ , however, despite the fact that the scheme is conservative, such non-negativity conditions are not immediately forthcoming. A related issue is the existence and uniqueness of numerical solutions—these properties can be ensured when  $\alpha = \beta = 1$ , as can easily be deduced from the update form (3.32), but otherwise are not immediately apparent.

At the level of the von Kármán system itself, due to the disparity between wave speeds, even in the linear case, between the longitudinal and transverse motions, the variables  $\mathbf{u}$  should be treated distinctly (using either distinct time steps or distinct grids) in order to achieve the best numerical behaviour (i.e., the least anomalous numerical dispersion). This issue has not been addressed in this article, but it is hoped that the construction techniques employed here can be extended to handle such cases.

Finally, all the schemes presented here are implicit, including the useful special case of  $\alpha = \beta = 1$ , and will require the solution of linear systems, which form the largest part of the computational load. Under small amplitude vibration conditions, the linear systems to be solved are diagonally dominant, and relatively simple and efficient methods (such as, e.g., Jacobi methods [53]) may be used; at higher amplitudes, however, the diagonal dominance property is lost, and one must revert to more general (and computationally costly) methods, such as, e.g., conjugate gradient techniques. Simple conditions on the range of vibration amplitudes which guarantee diagonal dominance would be of great interest. On top of this, though numerical energy is conserved in infinite precision, finite wordlength effects lead to a deterioration of the energy conservation property. For very large vibration amplitudes, one should expect that the linear systems to be solved will be poorly-conditioned, and thus one will see greater variation in the numerical energy, leading, ultimately, to instability due to truncation effects. In the present case, however, it appears that such vibration amplitudes greatly exceed the conditions for validity of the von Kármán model itself, and thus the family of schemes presented here should be safe to use under realistic conditions.

## VII. ACKNOWLEDGMENTS

This work was supported by the European Research Council, under grant StG-2011-279068-NESS.

## APPENDIX: ROTATORY INERTIA AND LOSS

If effects of rotatory inertia and loss are included, the dynamic equations (2.1a) and (2.1b), in dimensionless form, may be augmented to

$$\ddot{\mathbf{u}} - \operatorname{div} \mathbf{N} + \sigma_{\mathbf{u}} \dot{\mathbf{u}} = 0 \quad (7.1a)$$

$$\ddot{w} - \Delta \ddot{w} - \operatorname{div} \operatorname{div} \mathbf{M} - \operatorname{div} (\mathbf{N} \nabla w) + \sigma_w \dot{w} = 0 \quad (7.1b)$$

where the terms involving  $\sigma_{\mathbf{u}} \geq 0$  and  $\sigma_w \geq 0$  allow for simple loss.

In this case, the energy conservation equation (7.2) becomes

$$\frac{d}{dt}\mathcal{H}' = -\mathcal{Q} \quad (7.2)$$

where

$$\mathcal{H}' = \mathcal{H} + \frac{1}{2}\|\nabla\dot{w}\|^2 \geq 0 \quad \mathcal{Q} = \sigma_{\mathbf{u}}\|\dot{\mathbf{u}}\|^2 + \sigma_w\|\dot{w}\|^2 \geq 0 \quad (7.3)$$

The system is thus dissipative, so that  $0 \leq \mathcal{H}'(t) \leq \mathcal{H}'(0)$ , for  $t \geq 0$ .

Similarly, scheme (3.14) may be augmented as

$$\delta_{tt}\mathbf{u} - \operatorname{div} \left( \hat{\mathbf{N}}_{\mathbf{u}} + \hat{\mathbf{N}}_w \right) + \sigma_{\mathbf{u}}\delta_t.\mathbf{u} = 0 \quad (7.4a)$$

$$\delta_{tt}w - \delta_{tt}\Delta w - \operatorname{div} \operatorname{div} \mathbf{M} - \operatorname{div} \left( \bar{\mathbf{N}}_{\mathbf{u}}\nabla\tilde{w} + \bar{\mathbf{N}}_w\nabla\tilde{w} \right) + \sigma_w\delta_t.w = 0 \quad (7.4b)$$

where the centered time difference operator  $\delta_t.$ , as defined in (3.2) has been employed.

The semi-discrete conservation equation (3.26) then becomes

$$\delta_{t+}\mathcal{H}' = -\mathcal{Q} \quad (7.5)$$

where

$$\mathcal{H}' = \mathcal{H} + \frac{1}{2}\|\delta_{t-}\nabla w\|^2 \geq 0 \quad \mathcal{Q} = \sigma_{\mathbf{u}}\|\delta_t.\mathbf{u}\|^2 + \sigma_w\|\delta_t.w\|^2 \geq 0 \quad (7.6)$$

The semi-discrete system is thus also dissipative, so that  $0 \leq \mathcal{H}'^n \leq \mathcal{H}'^0$ , for time steps  $n \geq 0$ .

## REFERENCES

1. N. Yamaki. Influence of large amplitudes on flexural vibrations of elastic plates. *Zeitschrift für Angewandte Mathematik und Mechanik*, 41:501–510, 1961.
2. G.C. Kung and Y.H. Pao. Nonlinear flexural vibration of a clamped circular plate. *Journal of Applied Mechanics*, 39:1050–1054, 1972.
3. A. H. Nayfeh and D. T. Mook. *Nonlinear oscillations*. John Wiley & Sons, New-York, 1979.
4. S. Sridhar, D. T. Mook, and A. H. Nayfeh. Non-linear resonances in the forced responses of plates, part I: symmetric responses of circular plates. *Journal of Sound and Vibration*, 41(3):359–373, 1975.
5. J. Hadian and A.H. Nayfeh. Modal interaction in circular plates. *Journal of Sound and Vibration*, 142:279–292, 1990.
6. S.I. Chang, A.K. Bajaj, and C.M. Krousgrill. Non-linear vibrations and chaos in harmonically excited rectangular plates with one-to-one internal resonance. *Non-linear Dynamics*, 4:433–460, 1993.
7. C. Touzé, O. Thomas, and A. Chaigne. Asymmetric non-linear forced vibrations of free-edge circular plates, part I: theory. *Journal of Sound and Vibration*, 258(4):649–676, 2002.
8. O. Thomas, C. Touzé, and A. Chaigne. Asymmetric non-linear forced vibrations of free-edge circular plates, part II: experiments. *Journal of Sound and Vibration*, 265(5):1075–1101, 2003.
9. M. Amabili. Theory and experiments for large-amplitude vibrations of rectangular plates with geometric imperfections. *Journal of Sound and Vibration*, 291(3-5):539–565, 2006.

10. M. Amabili. *Nonlinear vibrations and stability of shells and plates*. Cambridge University Press, 2008.
11. M. Ducceschi, C. Touzé, S. Bilbao, and C.J. Webb. Nonlinear dynamics of rectangular plates: investigation of modal interaction in free and forced vibrations. *Acta Mechanica*, 225(1):213–232, 2014.
12. C. Touzé, O. Thomas, and M. Amabili. Transition to chaotic vibrations for harmonically forced perfect and imperfect circular plates. *International Journal of Non-linear Mechanics*, 46(1):234–246, 2011.
13. C. Touzé, S. Bilbao, and O. Cadot. Transition scenario to turbulence in thin vibrating plates. *Journal of Sound and Vibration*, 331(2):412–433, 2012.
14. J. Awrejcewicz and V. A. Krysko. Feigenbaum scenario exhibited by thin plate dynamics. *Nonlinear Dynamics*, 24:373–398, 2001.
15. J. Awrejcewicz, V. A. Krysko, and A. V. Krysko. Spatio-temporal chaos and solitons exhibited by von Kármán model. *International Journal of bifurcation and Chaos*, 12(7):1465–1513, 2002.
16. I. Chueshov and I. Lasiecka. Inertial manifolds for von Kármán plate equations. *Applied Mathematics and optimization*, 46:179–206, 2002.
17. I. Chueshov and I. Lasiecka. Attractors and long time behavior of von Kármán thermoelastic plates. *Applied Mathematics and optimization*, 58:195–241, 2008.
18. G. Düring, C. Josserand, and S. Rica. Weak turbulence for a vibrating plate: Can one hear a Kolmogorov spectrum? *Physical Review Letters*, 97:025503, 2006.
19. A. Boudaoud, O. Cadot, B. Odille, and C. Touzé. Observation of wave turbulence in vibrating plates. *Physical Review Letters*, 100:234504, 2008.
20. N. Mordant. Are there waves in elastic wave turbulence ? *Physical Review Letters*, 100:234505, 2008.
21. B. Miquel and N. Mordant. Nonlinear dynamics of flexural wave turbulence. *Phys. Rev. E*, 84:066607, 2011.
22. T. Humbert, O. Cadot, G. Düring, C. Josserand, S. Rica, and C. Touzé. Wave turbulence in vibrating plates: The effect of damping. *EPL (Europhysics Letters)*, 102(3):30002, 2013.
23. N. Yokoyama and M. Takaoka. Weak and strong wave turbulence spectra for elastic thin plate. *Phys. Rev. Lett.*, 110:105501, 2013.
24. B. Miquel, A. Alexakis, C. Josserand, and N. Mordant. Transition from wave turbulence to dynamical crumpling in vibrated elastic plates. *Phys. Rev. Lett.*, 111:054302, 2013.
25. M. Ducceschi, O. Cadot, C. Touzé and S. Bilbao. Dynamics of the wave turbulence spectrum in vibrating plates: A numerical investigation using a conservative finite difference scheme. *Physica D*, 280–281:73–85, 2014.
26. T. von Kármán. Festigkeitsprobleme im maschinenbau. *Encyklopedie der Mathematischen Wissenschaften*, 4(4):311–385, 1910.
27. H-N Chu and G. Herrmann. Influence of large amplitudes on free flexural vibrations of rectangular elastic plates. *Journal of Applied Mechanics*, 23:532–540, 1956.
28. C.Y. Chia. *Nonlinear Analysis of Plates*. McGraw Hill, New-York, 1980.
29. O. Thomas and S. Bilbao. Geometrically nonlinear flexural vibrations of plates: In-plane boundary conditions and some symmetry properties. *Journal of Sound and Vibration*, 315(3):569–590, 2008.
30. A. Föppl. *Vorlesungen über technische Mechanik*. Druck und Verlag von B.G. Teubner, Leipzig, 1907.

31. L.D. Landau and E.M. Lifschitz. *Theory of Elasticity*. Elsevier Butterworth Heinemann, 1986. third edition.
32. Z.P. Bazant and L. Cedolin. *Stability of structures*. World Scientific, Singapore, 2010. third edition.
33. Z. Yosibash and R.M. Kirby. Dynamic response of various von Kármán non-linear plate models and their 3-d counterparts. *International Journal of Solids and Structures*, 42:2517–2531, 2005.
34. M. Amabili. A comparison of shell theories for large-amplitude vibrations of circular cylindrical shells: Lagrangian approach. *Journal of Sound and Vibration*, 264:1091–1125, 2003.
35. S. Bilbao. A family of conservative finite difference schemes for the dynamical von Kármán plate equations. *Numerical Methods for Partial Differential Equations*, 24(1):193–216, 2008.
36. P. Ribeiro and M. Petyt. Nonlinear vibration of plates by the hierarchical finite element and continuation methods. *International Journal of Mechanical Sciences*, 41(45):437 – 459, 1999.
37. P. Ribeiro. Non-linear forced vibrations of thin/thick beams and plates by the finite element and shooting methods. *Computers and Structures*, 82(1719):1413 – 1423, 2004.
38. F. Boumediene, A. Miloudi, J.M. Cadou, L. Duigou, and E.H. Boutyour. Nonlinear forced vibration of damped plates by an asymptotic numerical method. *Computers and Structures*, 87(2324):1508 – 1515, 2009.
39. C. Touzé, M. Vidrascu, and D. Chapelle. Direct finite element computation of non-linear modal coupling coefficients for reduced-order shell models. *Computational Mechanics*, accepted for publication, 2014.
40. R.M. Kirby and Z. Yosibash. Solution of von Kármán dynamic non-linear plate equations using a pseudo-spectral method. *Computer Methods in Applied Mechanics and Engineering*, 193:575–599, 2004.
41. J.C. Simo, N. Tarnow, and K.K. Wong. Exact energy-momentum conserving algorithms and symplectic schemes for nonlinear dynamics. *Computer Methods in Applied Mechanics and Engineering*, 100(1):63 – 116, 1992.
42. J. C. Simo and N. Tarnow. A new energy and momentum conserving algorithm for the non-linear dynamics of shells. *International Journal for Numerical Methods in Engineering*, 37(15):2527–2549, 1994.
43. E. Hairer, C. Lubich, and G. Wanner. *Geometric Numerical Integration: Structure-preserving Algorithms for Ordinary Differential Equations*. Springer, 2006. second edition.
44. R. McLachlan. Symplectic Integration of Hamiltonian Wave Equations. *Numerische Mathematik*. 66:465–92, 1994.
45. A. Nayfeh and P. Pai. *Linear and Nonlinear Structural Mechanics*. John Wiley and Sons, 2004.
46. S. Lukasiewicz. *Local loads in plates an shells*. Sijthoff and Noordhoff, Alphenaan der Rijn, 1979.
47. J. Reddy. *Mechanics of Laminated Composite Plates*. CRC Press, 2004.
48. C. Chia. *Nonlinear Analysis of Plates*. McGraw Hill, 1980.
49. D. Tataru and M. Tucsnak. On the Cauchy problem for the full von Kármán system. *Nonlinear Differential Equations and Applications*, 4:325–340, 1997.
50. K. Graff. *Wave Motion in Elastic Solids*. Dover, New York, New York, 1975.
51. L. Trefethen. *Spectral Methods in Matlab*. SIAM, Philadelphia, Pennsylvania, USA, 2000.

52. Supplementary Matlab code is available at  
<http://www.ness-music.eu/wp-content/uploads/2015/02/nmpdematlab.zip>.
53. J. Strikwerda. *Finite Difference Schemes and Partial Differential Equations*. Wadsworth and Brooks/Cole Advanced Books and Software, Pacific Grove, California, 1989.

TABLE I. Calculated numerical energy values, for different values of the initial condition amplitude  $a$ , and for particular values of the time step  $n$ , using a finite difference discretization. Here, the time step is chosen as  $k = 1/20$ .

| $n$  | $a = 0.01$                         | $a = 1$           | $a = 5$                         |
|------|------------------------------------|-------------------|---------------------------------|
| 1    | $1.941538876811134 \times 10^{-4}$ | 2.093504501191837 | $1.435261060075711 \times 10^2$ |
| 2    | $1.941538876811129 \times 10^{-4}$ | 2.093504501191842 | $1.435261060075714 \times 10^2$ |
| 3    | $1.941538876811128 \times 10^{-4}$ | 2.093504501191841 | $1.435261060075717 \times 10^2$ |
| 4    | $1.941538876811132 \times 10^{-4}$ | 2.093504501191845 | $1.435261060075721 \times 10^2$ |
| 1000 | $1.941538876811936 \times 10^{-4}$ | 2.093504501194523 | $1.435261060076516 \times 10^2$ |

TABLE II. Calculated numerical energy values, for different values of the initial condition amplitude  $a$ , and for particular values of the time step  $n$ , using a Fourier discretization. Here, the time step is chosen as  $k = 1/20$ .

| $n$  | $a = 0.01$                         | $a = 1$           | $a = 5$                         |
|------|------------------------------------|-------------------|---------------------------------|
| 1    | $1.948149596712886 \times 10^{-4}$ | 2.100321257296917 | $1.438201589955981 \times 10^2$ |
| 2    | $1.948149596712884 \times 10^{-4}$ | 2.100321257296906 | $1.438201589955980 \times 10^2$ |
| 3    | $1.948149596712904 \times 10^{-4}$ | 2.100321257296910 | $1.438201589955976 \times 10^2$ |
| 4    | $1.948149596712887 \times 10^{-4}$ | 2.100321257296918 | $1.438201589955981 \times 10^2$ |
| 1000 | $1.948149596712743 \times 10^{-4}$ | 2.100321257296243 | $1.438201589955047 \times 10^2$ |